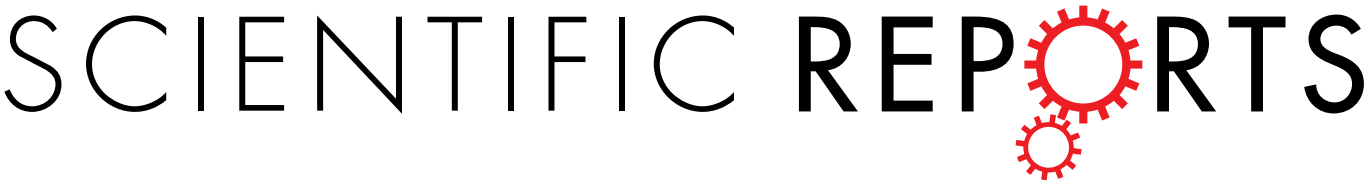

OPEN

Anisotropic magnetotransport and extremely large magnetoresistance in $NbAs_2$ single crystals

Received: 15 January 2018
Accepted: 5 April 2018
Published online: 23 April 2018

G. Peramaiyan[1], Raman Sankar[1,2], I. Panneer Muthuselvam[1,2,3] & Wei-Li Lee[1]

We report the extremely large magnetoresistance and anisotropic magnetoresistance in a non-magnetic semimetallic $NbAs_2$ single crystal. Unsaturated transverse XMR with quadratic field dependence has been observed to be ~3×10^5 % at 2 K and 15T. Up to 12.5 K, clear Shubnikov de Haas (SdH) quantum oscillations were observed from which two distinct Fermi pockets were identified. The corresponding quantum electronic parameters such as effective cyclotron mass and Dingle temperature were obtained using Lifshitz-Kosevich formula. From the field dependent Hall resistivity at 2 K, carrier concentrations $n_e(n_h) = 6.7691\ (6.4352) \times 10^{25}\ m^{-3}$ and mobilities $\mu_e\ (\mu_h) = 5.6676\ (6.6947)\ m^2 V^{-1} s^{-1}$ for electrons (e) and holes (h) were extracted using semiclassical two-band model fitting. We observed large anisotropic magnetoresistance about 84%, 75%, and 12% at 0.75T and 6 K for three different orientations γ, θ and ϕ, respectively, similar to that in several topological semimetallic systems. Magnetic properties of $NbAs_2$ are similar to the case of graphite, without any phase transition in the temperature range from 5 K to 300 K.

Exploration of novel states of quantum matter with exotic physical phenomena is one of the new frontiers in condensed matter physics. Unusual transport properties such as large magnetoresistance (MR) not only provide signatures of unique states of matter but also play a vital role in device applications such as magnetic field sensors, random access memories, hard drives, spintronic devices, etc[1–3]. The unsaturated large magnetoresistance with quadratic field (H^2) dependence, transverse and longitudinal linear magnetoresistance in nonmagnetic semimetals are unusual phenomena, and its origin is under debate in condensed matter physics. In some semimetals such as $NbSb_2$[4], LaSb[5] and LaBi[6], the origin of large unsaturated MR with H^2 is attributed to the electron-hole compensation. On the other hand, the electron-hole compensation with H^2 of MR and linear MR at intense high fields are observed in the topological semimetals such as a Dirac semimetal, ZrSiS[7] and a Weyl semimetal TaAs[8], but its origin is different from those aforementioned materials[9]. Among the family of nonmagnetic semimetallic systems, $NbAs_2$ crystallizes in monoclinic with inversion center ($C12/m1$)[10], and is demonstrated to exhibit large MR with H^2 dependence[10–13]. First principle calculations revealed that the $NbAs_2$ system possesses four types of Fermi surfaces[11]. It is reported that the $NbAs_2$ single crystal shows unsaturated large transverse MR about 8000 at 9 T and 1.8 K[11], 8800 at 9 T and 2 K[12], 1000 at 14 T and 2.5 K[13] and ultra-high mobility of the order of $10^4 - 10^5\ cm^2 V^{-1} s^{-1}$, and its origin is attributed to electron-hole compensation. The field induced XMR with metal-insulator-like cross-over behavior followed by a resistivity plateau has been observed in a nonmagnetic semimetallic system $NbAs_2$[12,13], where nontrivial Berry phase[13] and negative longitudinal MR[11] have also been observed. However, the detailed angle dependent magnetoresistance study will help to understand the anisotropic properties of $NbAs_2$, which has not been fully studied. In this work, we report a systematic study of anisotropic magnetoresistance (AMR) in $NbAs_2$ crystal. Large AMR in $NbAs_2$ may be linked to the non-trivial Berry phase of topological systems. High magnetic field transport measurement in the $I \perp H$ geometry shows the large unsaturated parabolic MR. The results of fitting with a semiclassical two-band model reveal electron-hole compensation with temperature dependent mobility in $NbAs_2$.

[1]Institute of Physics, Academia Sinica, Taipei, 10617, Taiwan. [2]Center for Condensed Matter Sciences, National Taiwan University, Taipei, 10617, Taiwan. [3]Department of Materials Science, Central University of Tamil Nadu, Neelakudi, Thiruvarur, 610005, Tamil Nadu, India. Correspondence and requests for materials should be addressed to R.S. (email: sankarndf@gmail.com)

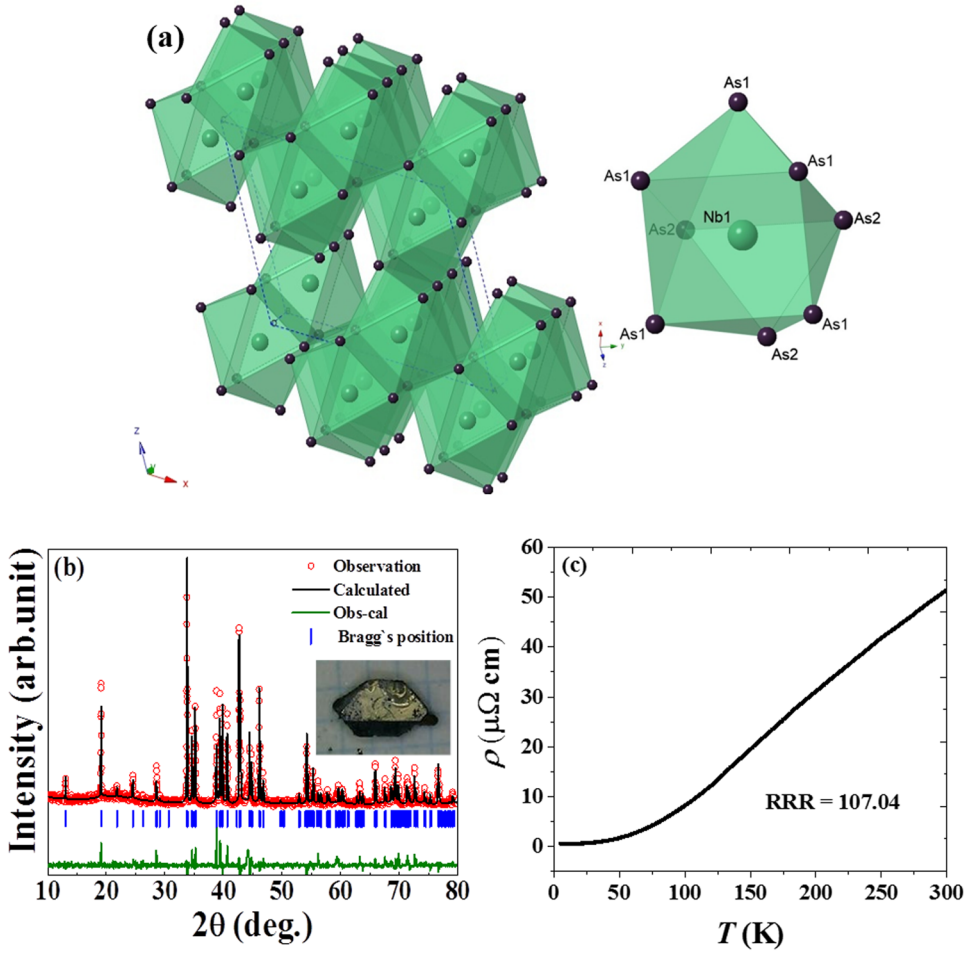

Figure 1. (**a**) Crystal structure of $NbAs_2$. The inset shows the triangular prism of $NbAs_2$ where a Nb (Nb1) atom is bounded by six As (As1, As2) atoms and two As atoms lie outside the rectangular faces. (**b**) Powder X-ray diffraction (XRD) pattern and Rietveld refinement results of for pulverized $NbAs_2$ single crystals. The inset shows the as-grown single crystal of $NbAs_2$. (**c**) shows the temperature dependence of resistivity with metallic profile, RRR about 107.04.

Results and Discussion

$NbAs_2$ crystallizes in a monoclinic system with the centrosymmetric space group of C12/*m*1. It belongs to a larger family of transition metal dipnictides MPn_2 (M = V, Nb, Ta, Cr, Mo, and W, Pn = P, As and Sb), which is found to crystallize in $OsGe_2$ structure type. In the $NbAs_2$ crystal structure (as shown in Fig. 1(a) and its inset), each Nb (Nb1) atom is bounded by six As (As1, As2) atoms and two As atoms lie outside the rectangular faces. Figure 1(b) shows the Rietveld refinement of the X-ray powder diffraction results (Bruker D8) using Cu-K_α radiation for the pulverized crystalline sample of $NbAs_2$. The inset of Fig. 2(a) shows the as-grown single crystals of $NbAs_2$. The refined lattice parameters, $a = 9.3560$ (2) Å, $b = 3.3828$ (1) Å, $c = 7.7966(2)$ Å, and $\beta = 119.440(15)°$, are in good agreement with those reported in the literature[10].

Figure 2(a) shows the plot of resistivity as a function of magnetic field at various temperatures measured in the $I \perp H$ configuration. The data obtained by sweeping the magnetic field from 15 T to −15T were then symmetrized using $\rho(H) = [\rho(H) + \rho(-H)]/2$. $NbAs_2$ exhibits quite large magnetoresistance (MR) at low temperatures with a strong Shubnikov de Haas (SdH) quantum oscillation and quadratic field dependence as shown in Fig. 2(b). The MR percentage calculated from $[(\rho(H) - \rho(0))/\rho(0)] \times 100\%$, reaches 303,200% at 2 K without any signature of saturation in a field of 15 T. It is observed that the MR of $NbAs_2$ is very sensitive with respect to sample quality, since sample-1 shows MR about 115,200% at 2 K and 9 T with a residual resistivity ratio (RRR = ρ_{300K}/ρ_{3K}) of 107.04 (Fig. 1(c)), whereas the MR of sample 2 shows 170,800% with a RRR of about 110.49 as shown in Fig. S1. The RRR of $NbAs_2$ crystals attest to the good metallicity and quality of the grown crystals, which is comparable to that reported for the Weyl semimetal NbP (RRR = 115)[9], higher than those of TaAs (RRR = 49)[8] and NbAs (RRR = 72)[14], but lower than less than that previously reported for $NbAs_2$ (RRR = 222, and 317)[11,12] crystals. The unsaturated MR behavior of $NbAs_2$ is similar to the semimetals WTe_2[15] and $NbSb_2$[4]. The large and unsaturated MR of $NbAs_2$ is higher than that for the semimetals $NbSb_2$ (MR = 1.3×10^{5}% at 2 K and 9 T)[4], LaBi (MR = 0.38×10^{5}% at 2 K and 14 T)[6], the Dirac semimetals ZrSiS[7] (MR = 1.4×10^{5}% at 2 K and 9 T) and Cd_3As_2 (MR = 1.6×10^{5}% at 2.5 K and 15 T)[16]. It is comparable with that recently reported for $NbAs_2$ (8×10^{5}% at 9 T at

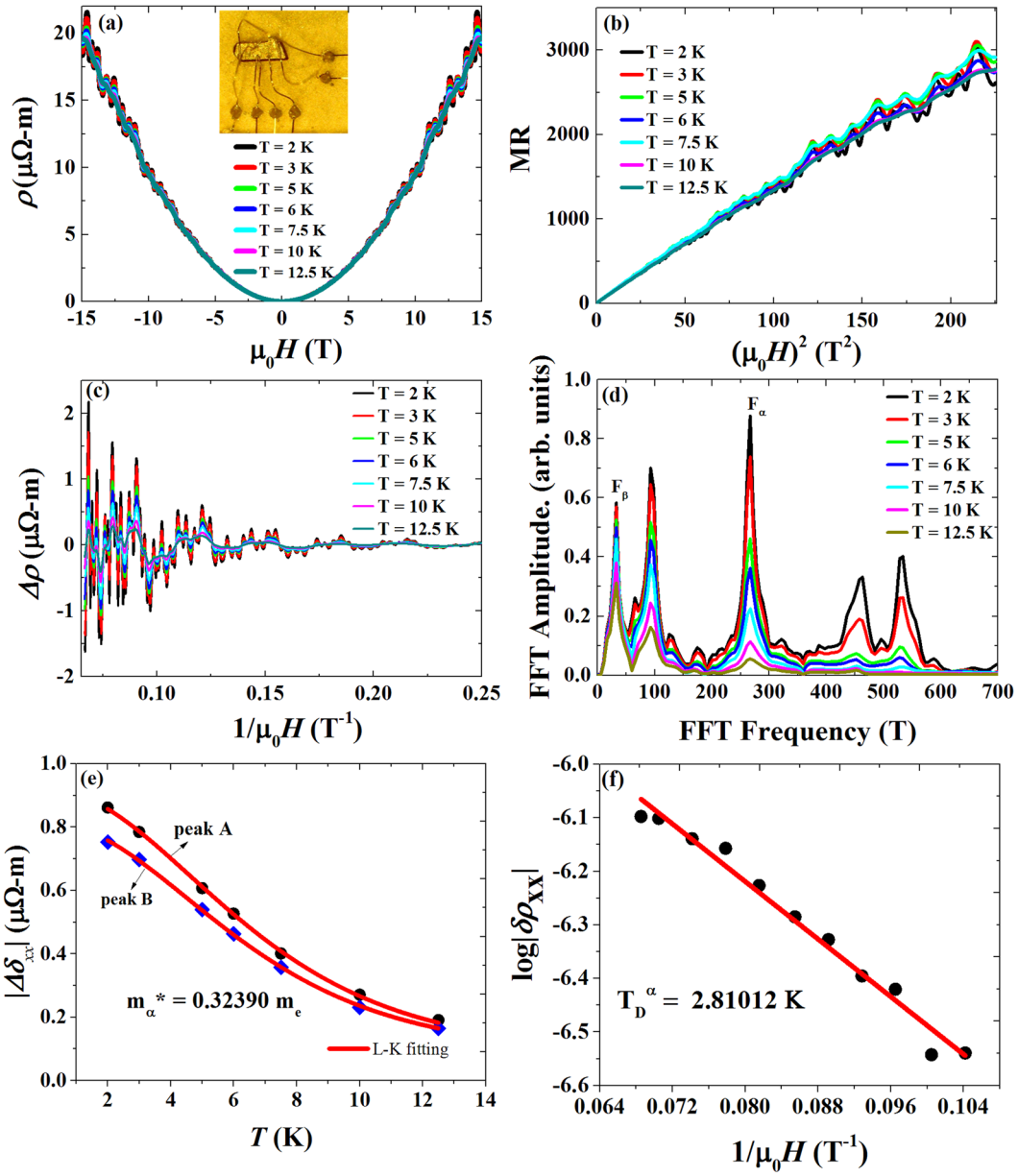

Figure 2. (**a**) Field dependence of resistivity ρ (H, T) of sample-1 along $I \perp H$ at various temperatures showing clear SdH quantum oscillations. The insets show the measurement geometry (left) and six-probe geometry for the simultaneous measurement of ρ_{xx} and ρ_{xy} (right). (**b**) It shows the quadratic field dependence of magnetoresistance MR = $[\rho(H) - \rho(0)]/\rho(0)]$ of sample −1. (**c**) Total resistivity oscillatory patterns $\Delta\rho_{xx}$ as a function of inverse magnetic field $(1/M\mu_0 H)$ at various temperatures for the $I \perp H$ geometry. (**d**) FFT spectrum of quantum oscillations showing two distinct peaks at $F_\alpha = 266$ T and $F_\beta = 32$ T as well as their harmonics for various temperatures. (**e**) Temperature dependence of oscillation amplitude at fixed magnetic field for the observed Fermi pocket. Peak A&B represent the positions of resistivity oscillatory amplitudes. The solid line is the L-K fitting, used to extract the effective cyclotron mass and Dingle temperature. (**f**) It shows the log $|\Delta\rho_{xx}|$ vs T plot at 3 K, and linear fitting yields the Dingle temperature.

1.8 K[11], $1 \times 10^{5\%}$ at 14 T at 2.5 K[13]), the topological semimetal LaSb (9×10^5% at 9 T and 2 K)[17] and the Weyl semimetal candidates NbP ($8.5 \times 10^{5\%}$ at 9 T at 1.85 K)[9] and NbAs (MR = 2.3×10^5% at 9 T and 2 K)[14]. In order to analyse the SdH quantum oscillations, the second order polynomial smoothed background was subtracted from the field dependent resistivity, $\rho(H)$. Figure 2(c) shows the total oscillatory pattern ($\Delta\rho$) with obvious quantum oscillations starting from 4 T as a function of inverse magnetic field $(1/\mu_0 H)$ for $(I \perp H)$ geometry. From the fast Fourier transformation spectrum (FFT) as shown in Fig. 2(d), two major peaks are observed at $F_\alpha = 266$ T and $F_\beta = 32$ T as well as their harmonics, where α and β are denoted as high and low frequency peaks, respectively. Since the amplitude of total oscillation ($\Delta\rho_{xx}$) seems to show complex periodic behavior, FFT frequency filtering was used to extract the respective oscillation patterns denoted as ($\delta\rho$) for the observed frequency of 266 T to

estimate the cyclotron effective mass (m^*) and Dingle temperature (T_D) as shown in Fig. S2(b). From the Onsager relation $F = (\phi_0/2\pi^2)A_F$, where the A_F is the extremal Fermi surface cross-sectional area perpendicular to the field, F is the frequency of the oscillation, and ϕ_0 is the magnetic flux quantum. The Fermi surface cross sections are calculated to be 25.3×10^{-3} Å^{-2} and 3.04×10^{-3} Å^{-2} for 266 T and 32 T, respectively. The total oscillatory pattern ($\Delta\rho$) can be expressed based on the Lifshitz-Kosevich (L-K) formalism[18]

$$\Delta\rho(T, B) = \exp[-X(T_D, B)]\frac{X(T, B)}{\sinh[X(T, B)]}\Delta\rho' \quad (1)$$

where $\Delta\rho'$ is the oscillatory component without damping, and $X(T, B) = 2\pi^2 k_B T m^*/\hbar eB$. Here, m^* refers to the effective cyclotron mass, and T_D is the Dingle temperature. The temperature dependence of $\delta\rho$ is fitted well with the L-K formula as shown in Fig. 2(e). The fitting results yield the effective cyclotron mass $m_\alpha^* = 0.323 \pm 0.00090 m_e$, where m_e is the electron rest mass. Figure 2(f) shows the fitting results of the respective $\delta\rho$ for various inverse fields ($1/\mu_0 H$) at a fixed temperature of 3 K, which yields the Dingle temperature $T_D^\alpha = 2.810 \pm 0.004\ K$. From the Dingle temperature, the single particle scattering rate is calculated to be $\tau_s = \frac{\hbar}{2\pi k_B T_D} = 4.35 \times 10^{-13}$ s. The obtained results of $NbAs_2$ are consistent with previous studies[11–13].

The anisotropic magnetoresistance (AMR) is measured along three different field orientations of γ, θ and ϕ at different field strengths from 0.1 T to 0.75 T as shown in Fig. 3(a,c,e). The inset of Fig. 3(b) shows the AMR measurement geometry for the γ, θ and ϕ orientations. The AMR effect for the γ orientation is presented in Fig. 3(a) as a polar plot, which illustrates the two-fold symmetry with a variation of period π. In this configuration, the magnitude of AMR reaches a maximum about 75% at $\gamma = 10°$ and minium about 32% at $\gamma = 100°$ for the field of 0.75 T and temperature of 6 K, and a similar trend continues in the opposite way up to 180°. In the ϕ orientation, the magnitude of AMR shows a minimum about 12% at $\phi = 0°$ when the current is parallel to H, and maximum about 29.5% at $\phi = 90°$ when the current is perpendicular to H. The magnitudes of AMR are observed to be 75% and 12% for $I \perp H$ ($\theta = 0°$) and $I \| H$ ($\theta = 90°$), respectively, in the θ orientation. From the field dependent AMR measurements in three different orientations, it is clear that the AMR is positive, and its maximum always appears when the current is perpendicular to H. In order to analyse the power law dependence of MR, a double-logarithmic value between H and MR was taken for γ, θ and ϕ orientations as shown in Fig. 3(b,d,f), and the linear fitting of these plots yield the different slopes (m values) at various angles. The slope (m) varies from 1.233 at 0° to 1.632 at 90° for γ orientation. In the θ orientation, m values are found to be 1.260 at $\theta = 0°$ ($I \perp H$) and 1.201 $\theta = 90°$ ($I \| H$). For in-plane orientation (ϕ), m varies from 1.175 at $\phi = 0°$ to m = 1.743 at $\phi = 90°$. It is noteworthy that the power law dependence of MR is close to 1 particularly at $\phi = 0°$ and $\theta = 90°$ with $I \| H$ orientation. We also remark that the behavior of AMR with two-fold symmetry for γ and θ orientations remains the same regardless of the magnetic field strengths up to 0.75 T, whereas, for ϕ orientation, the two-fold symmetry in AMR gradually faded away in low field regime. The response of the charge carriers to the rotating magnetic field of magnitude about 0.75 T for three different orientations is studied as a function of temperature as shown in Fig. 4(a–c). The variation of AMR, $\Delta\rho 1 = [\rho_{peak} - \rho_{valley}]/\rho_{valley}$, with respect to temperature is presented in Fig. 4(d) for three different orientations. From the temperature dependence of magnetoresistance, AMR increases with decreasing temperature, and it is almost saturated at low temperatures. The two-fold symmetry is well pronounced at low temperature (6 K), and it is sustained up to a measured temperature of 150 K.

Since the MR value of conventional metals is usually small in magnitude and saturated at high fields, and the consequences of unsaturated XMR and ultrahigh mobility in nonmagnetic topological semimetals such as Cd_3As_2[16], TaAs, etc, is related to Dirac and Weyl fermions (topological surface states and linear band dispersion), the fact that $NbAs_2$ exhibits unsaturated XMR is extremely important. In order to identify the intrinsic magnetic property of $NbAs_2$, magnetization measurements as a function magnetic field and temperature were carried as shown in Fig. 5(a,b). The linear field dependence of magnetization in $NbAs_2$ is similar to that observed for graphite[19,20]. Even though a sudden rise of magnetization below 25 K due to small amount of magnetic impurities, there is no significant effect in the AMR behavior of $NbAs_2$.

In ferromagnetic metals, AMR typically shows the maximum resistivity when the current is parallel to magnetic field due to spin-orbit scattering, and minimum resisitivity when the current is perpenducular to magnetic field[21,22]. Since the $NbAs_2$ belongs to nonmagnetic material category, the physical origin of the AMR effect in the present system is thus different from that in magnetic materials.

According to the semiclassical two-band model[23,24], the total conductivity tensor is expressed in the complex form of

$$\hat{\sigma} = e\left[\frac{n\mu_n}{(1 + i\mu_n H)} + \frac{p\mu_p}{(1 - i\mu_p H)}\right], \quad (2)$$

where the $n(p)$ and $\mu_n(\mu_p)$ are electron (hole) concentration and electron (hole) mobility, respectively; e is the electron charge and 'H' is the magnetic field. The total conductivity is then expressed as

$$\hat{\sigma} = e\left[\left\{\frac{n\mu_n}{(1 + \mu_n^2 H^2)} + \frac{p\mu_p}{(1 + \mu_p^2 H^2)}\right\} + i\left\{\frac{-n\mu_n^2 H}{(1 + \mu_n^2 H^2)} + \frac{p\mu_p^2 H}{(1 + \mu_p^2 H^2)}\right\}\right] \quad (3)$$

In equation (2), the Re and Im $\hat{\sigma}$ equal to σ_{xx} and σ_{xy}, respectively where $\sigma_{xy} = \frac{\rho_{xy}}{\rho_{xy}^2 + \rho_{xx}^2}$ and $\sigma_{xx} = \frac{\rho_{xx}}{\rho_{xy}^2 + \rho_{xx}^2}$ and ρ_{xy} and ρ_{xx} are Hall and transverse resistivities, respectively. The magnetoresistance (MR) then follows

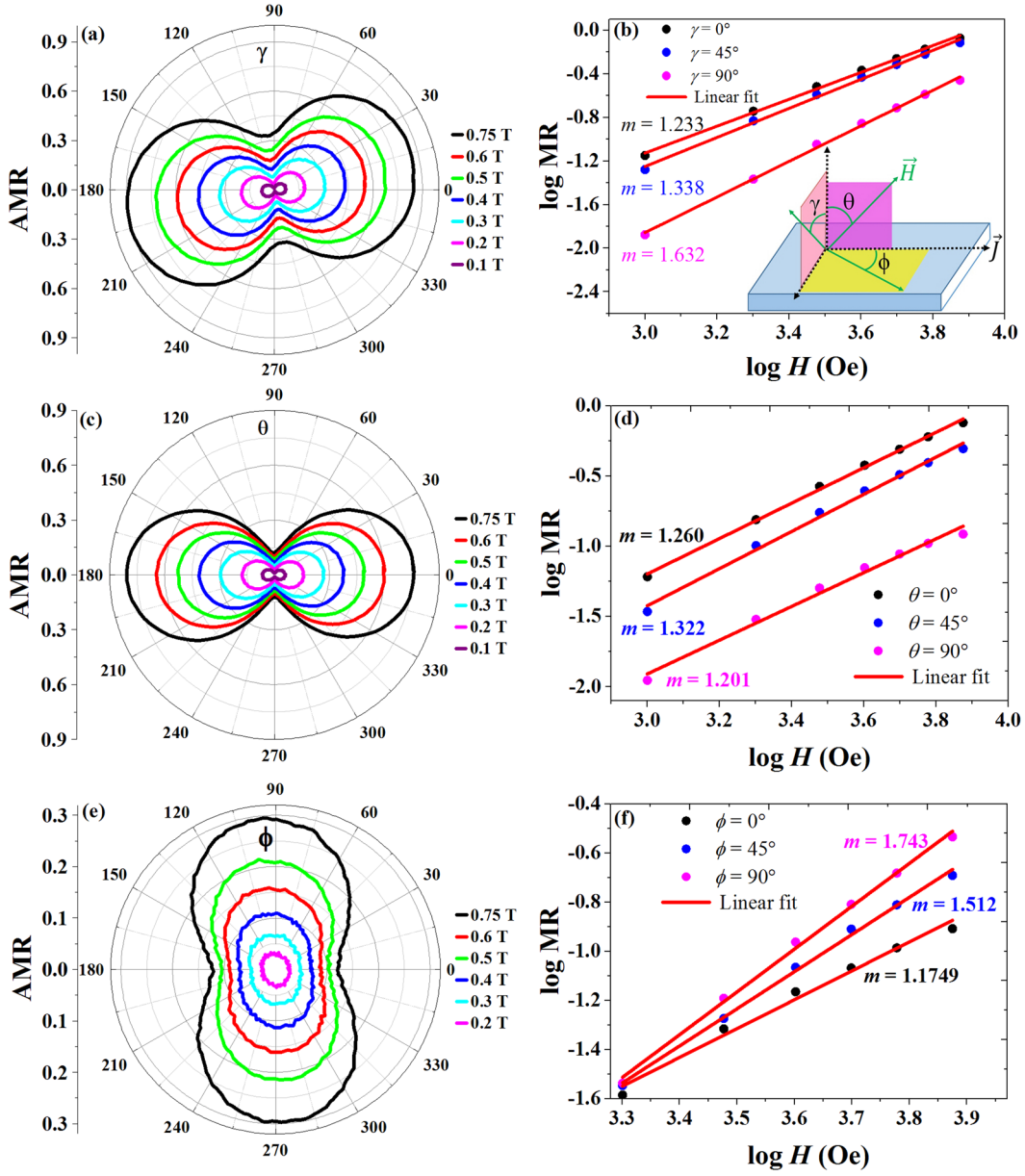

Figure 3. (**a**,**c**,**e**) show the polar plots of anisotropic magnetoresistance (AMR) for different magnetic field strengths from 0.1 T to 0.75 T at 6 K for γ, θ and ϕ orientations, respectively exhibiting the two-fold symmetry. (**b**,**d**,**f**) Plots of log (M.R.) vs log (H) shows the linear behavior. The solid lines are the linear fittings giving the slope (m) value, giving the order for field dependence. The insets show the definitions of γ, θ and ϕ within the measurement geometry.

$$MR = \frac{\rho(H) - \rho(0)}{\rho(0)} = \frac{n\mu_n p\mu_p(\mu_n + \mu_p)^2 H^2}{(n\mu_n + p\mu_p)^2 + ((n-p)\mu_n\mu_p H)^2} \tag{4}$$

From equation (2) n, p, μ_n and μ_p can be obtained by fitting the $\sigma_{xy}(H)$ data. For a perfect compensated system ($n = p$), MR follows a quadratic field dependence which is shown in Fig. 2(b). Figure 6(a) shows the Hall resistivity as a function of magnetic field with nonlinear behavior at low temperatures. The expanded view of ρ_{xy} below 1 T of H at 2 K is shown in the inset of Fig. 6(a). It is clear that the sign of ρ_{xy} changes from positive ($\rho_{xy} > 0$ in H < 0.4 T) to negative at high fields with nonlinear band, suggesting the multiband effect in the $NbAs_2$ system. At 200 K, ρ_{xy} shows positive value below 8 T of magnetic field as shown in Fig. S1(c) which suggests that holes dominate over electrons in the transport properties. By fitting the σ_{xy} data as shown in Fig. 6(b), carrier concentrations of $n = 6.7691 \times 10^{25}\,m^{-3}$ and $p = 6.4352 \times 10^{25}\,m^{-3}$, and mobilities of $\mu_p = 7.6947\,m^2\,V^{-1}\,s^{-1}$ and

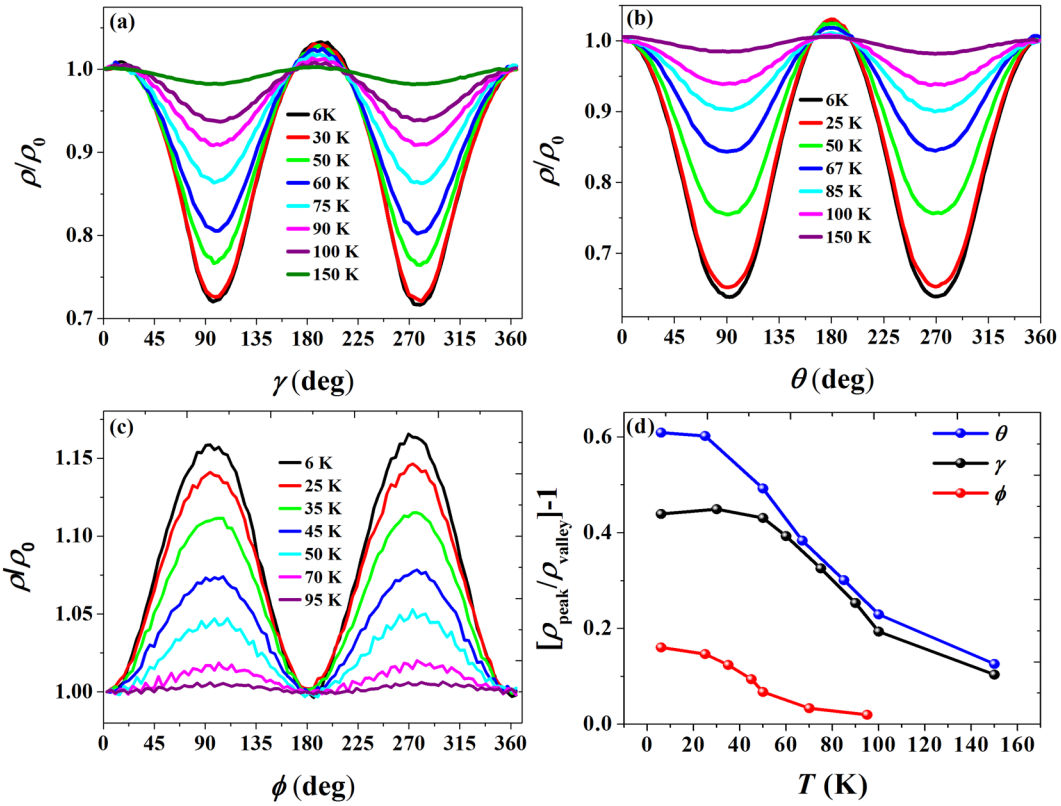

Figure 4. (**a**–**c**) show the normalized plots of temperature dependence of AMR measured at fixed magnetic field 0.75 T for γ (**a**), θ (**b**) and ϕ (**c**) orientations, respectively showing absence of phase transition up to the measured temperature range. (**d**) It shows the comparative plots of temperature dependence of magnetoresistance for three different orientations.

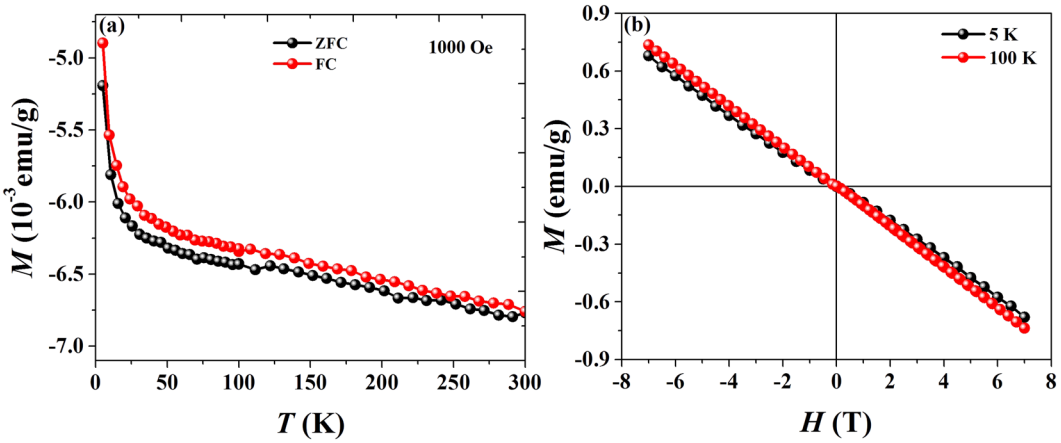

Figure 5. (**a**,**b**) show the *M*-*T* for 1000 Oe and *M*-*H* curves for 5 K and 100 K revealing the diamagnetic behavior in $NbAs_2$.

$\mu_n = 5.6676\ m^2\ V^{-1}\ s^{-1}$ at 2 K are extracted, as shown in Fig. 6(c). Figure 6(d) shows the ratio of *n* to *p* as the function of temperatures, suggesting that these two carriers are almost compensated in the $NbAs_2$ system.

The magnetic field and temperature dependent transport measurements revealed the highly compensated electron and hole pockets, which may be responsible for the observed XMR. Recently, the AMR effect is observed in several nonmagnetic materials such as ZrSiS[25], LaBi[26], WTe_2[27], etc,. For example, the AMR effect with the combination of two and four-fold symmetry and unsaturated MR with electron-hole compensation as well as open orbital of Fermi surface had been reported in a Dirac semimetal ZrSiS[28]. The large AMR may be regarded as the most promiment signature in transport for the non-zero Berry curvatures in topological systems[29]. The transport features of $NbAs_2$ we observed turn out to be similar to the Dirac semimetal ZrSiS[25] and WTe_2[27]. Further

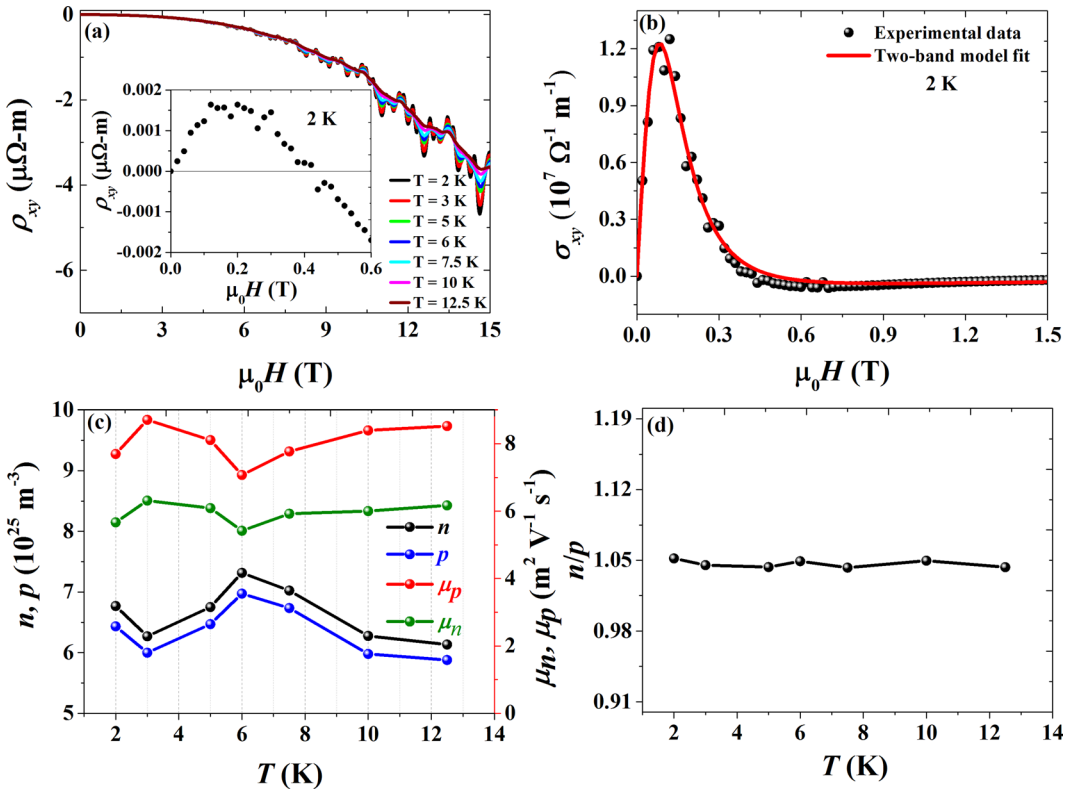

Figure 6. (**a**) Field dependence of the Hall resistivity (ρ_{xy}) at various temperatures. Inset shows the expanded view of ρ_{xy} in the low field region of about 0.6 T at 2 K. (**b**) Field dependence of the Hall conductivity at 2 K. The solid line is the fit of the two-band model giving the carrier concentrations and mobilities of electrons and holes. (**c**) Plot of carrier concentrations and mobilities of electrons and holes as a function of temperature. (**d**) The ratio of n to p as a function of temperature demonstrates the electron-hole compensation.

theoretical calculations and band structure characterizations are keenly required to reveal the possible nontrivial band topology in $NbAs_2$.

In summary, the single crystals of $NbAs_2$ were grown using the chemical vapour transport method. We observed extremely large, unsaturated and anisotropic MR in $NbAs_2$. Transverse magnetoresistance of $NbAs_2$ reaches a large value of about 303,200% at 2 K and 15 T, and MR follows a quadratic field dependence, which is in accord with the electron-hole compensation with the n/p ratio of about 1.05 determined from semiclassical two-band model fittings. From the SdH quantum oscillations, two distinct Fermi pockets were identified, and its effective electron mass and Dingle temperature were extracted from the L-K fitting. Interestingly, apparent two-fold symmetry and large magnitude in AMR are observed for three different field orientations, and power law dependence of MR is close to 1 for $I||H$ orientation. The origin of such large AMR effect in a non-magnetic semimetal $NbAs_2$ may be related to the presence of non-trivial Berry curvature in $NbAs_2$, where the magnetic contribution to the AMR effect has been excluded based on magnetization measurements.

Experimental Section

Sample preparation. Two step chemical vapor transport processes were used to synthesize and grow single crystals of $NbAs_2$. A quartz ampoule with a length of 30–40 cm was used for the synthesis and growth. At first, stoichiometric amounts of 5 N purity precursors of Nb and As in a molar ratio of 1:2 were sealed in an evacuated quartz ampoule. The vacuum-sealed quartz ampoule containing the binary mixture was treated at 950 °C for two days and then cooled to room temperature, yielding polycrystalline $NbAs_2$. Secondly, the polycrystalline powder of $NbAs_2$ was mixed with I_2 in a weight ratio of 100:1 and vacuum-sealed in a two-zone tube furnace having a thermal gradient of about 950-850 °C within ~40 cm. The resulting $NbAs_2$ single crystals have shiny surfaces with well-defined crystal facets as shown in the inset of Fig. 1(b).

References

1. Baibich, M. N. *et al.* Giant Magnetoresistance of (001)Fe/(001)Cr Magnetic Superlattices. *Phys. Rev. Lett.* **61**, 2472–2475 (1988).
2. Binasch, G., Grünberg, P., Saurenbach, F. & Zinn, W. Enhanced magnetoresistance in layered magnetic structures with antiferromagnetic interlayer exchange. *Phys. Rev. B* **39**, 4828–4830 (1989).
3. Daughton, J. M. GMR applications. *J. Magn. Magn. Mater.* **192**, 334–342 (1999).
4. Wang, K., Graf, D., Li, L., Wang, L. & Petrovic, C. Anisotropic giant magnetoresistance in NbSb2. *Sci. Rep.* **4**, 7328 (2014).
5. Zeng, L.-K. *et al.* Compensated Semimetal LaSb with Unsaturated Magnetoresistance. *Phys. Rev. Lett.* **117**, 127204 (2016).
6. Lei, S. S., Q., W., P.-J., G., K., L. & H. Large magnetoresistance in LaBi: origin of field-induced resistivity upturn and plateau in compensated semimetals. *New J. Phys.* **18**, 82002 (2016).

7. Singha, R., Pariari, A. K., Satpati, B. & Mandal, P. Large nonsaturating magnetoresistance and signature of nondegenerate Dirac nodes in ZrSiS. *Proc. Natl. Acad. Sci.* **114**, 2468–2473 (2017).
8. Zhang, C.-L. *et al*. Electron scattering in tantalum monoarsenide. *Phys. Rev. B* **95**, 85202 (2017).
9. Shekhar, C. *et al*. Extremely large magnetoresistance and ultrahigh mobility in the topological Weyl semimetal candidate NbP. *Nat Phys* **11**, 645–649 (2015).
10. Furuseth, S. & Kjekshus, A. The crystal structures of NbAs2 and NbSb2. *Acta Crystallogr.* **18**, 320–324 (1965).
11. Shen, B., Deng, X., Kotliar, G. & Ni, N. Fermi surface topology and negative longitudinal magnetoresistance observed in the semimetal NbAs2. *Phys. Rev. B* **93**, 195119 (2016).
12. Yuan, Z., Lu, H., Liu, Y., Wang, J. & Jia, S. Large magnetoresistance in compensated semimetals TaAs2 and NbAs2. *Phys. Rev. B* **93**, 184405 (2016).
13. Wang, Y.-Y., Yu, Q.-H., Guo, P.-J., Liu, K. & Xia, T.-L. Resistivity plateau and extremely large magnetoresistance in NbAs2 and TaAs2. *Phys. Rev. B* **94**, 41103 (2016).
14. Ronning, N. J. G. *et al*. Magnetotransport of single crystalline NbAs. *J. Phys. Condens. Matter* **27**, 152201 (2015).
15. Ali, M. N. *et al*. Large, non-saturating magnetoresistance in WTe2. *Nature* **514**, 205–208 (2014).
16. Liang, T. *et al*. Ultrahigh mobility and giant magnetoresistance in the Dirac semimetal Cd3As2. *Nat Mater* **14**, 280–284 (2015).
17. Tafti, F. F., Gibson, Q. D., Kushwaha, S. K., Haldolaarachchige, N. & Cava, R. J. Resistivity plateau and extreme magnetoresistance in LaSb. *Nat Phys* **12**, 272–277 (2016).
18. Shoenberg, D. *Magnetic Oscillations in Metals*. (Cambridge University Press, 1984).
19. Ramos, M. A. *et al*. Magnetic properties of graphite irradiated with MeV ions. *Phys. Rev. B* **81**, 214404 (2010).
20. Li, Z. *et al*. Field and temperature dependence of intrinsic diamagnetism in graphene: Theory and experiment. *Phys. Rev. B* **91**, 94429 (2015).
21. McGuire, T. & Potter, R. Anisotropic magnetoresistance in ferromagnetic 3d alloys. *IEEE Transactions on Magnetics* **11**, 1018–1038 (1975).
22. Rushforth, A. W. *et al*. Anisotropic Magnetoresistance Components in (Ga,Mn)As. *Phys. Rev. Lett.* **99**, 147207 (2007).
23. Ziman, J. M. *Electrons and Phonons: The Theory of Transport Phenomena in Solids*. (Oxford University Press, 2001).
24. N W. Ashcroft, N. D. M. *Solid State Physics*. (Saunders College, 1976).
25. Ali, M. N. *et al*. Butterfly magnetoresistance, quasi-2D Dirac Fermi surface and topological phase transition in ZrSiS. *Sci. Adv.* **2**, (2016).
26. Kumar, N. *et al*. Observation of pseudo-two-dimensional electron transport in the rock salt-type topological semimetal LaBi. *Phys. Rev. B* **93**, 241106 (2016).
27. Zhao, Y. *et al*. Anisotropic magnetotransport and exotic longitudinal linear magnetoresistance in WTe_2 crystals. *Phys. Rev. B* **92**, 41104 (2015).
28. Lv, Y.-Y. *et al*. Extremely large and significantly anisotropic magnetoresistance in ZrSiS single crystals. *Appl. Phys. Lett.* **108**, 244101 (2016).
29. Nandy, S., Sharma, G., Taraphder, A. & Tewari, S. Chiral Anomaly as the Origin of the Planar Hall Effect in Weyl Semimetals. *Phys. Rev. Lett.* **119**, 176804 (2017).

Acknowledgements

R.S. acknowledges the support provided by the Academia Sinica research program on Nanoscience and Nanotechnology under project number NM004 and Nanoscience and Nanotechnology Thematic Program of Academia Sinica. I.P.M. thanks Department of Science and Technology in India for the support of INSPIRE faculty Award No. DST/INSPIRE/04/2016/002275.

Author Contributions

R.S. and W.L.L. designed the study; R.S. synthesized and growth the sample; G.P., W.L.L. and I.P.M. performed transport measurements; all of the authors discussed the results and interpretations; G.P. wrote the manuscript, R.S. and W.L.L. revised the manuscript.

Additional Information

Supplementary information accompanies this paper at https://doi.org/10.1038/s41598-018-24823-z.

Competing Interests: The authors declare no competing interests.

Publisher's note: Springer Nature remains neutral with regard to jurisdictional claims in published maps and institutional affiliations.